Figure 13.26 Normalized response of InSb photodiodes in elevated temperature range. (From Wimmers, J. T., Davis, R. M., Niblack, C. A., and Smith, D. S., "Indium Antimonide Detector Technology at Cincinnati Electronics Corporation," *Proceedings of SPIE* 930, 125–38, 1988.)
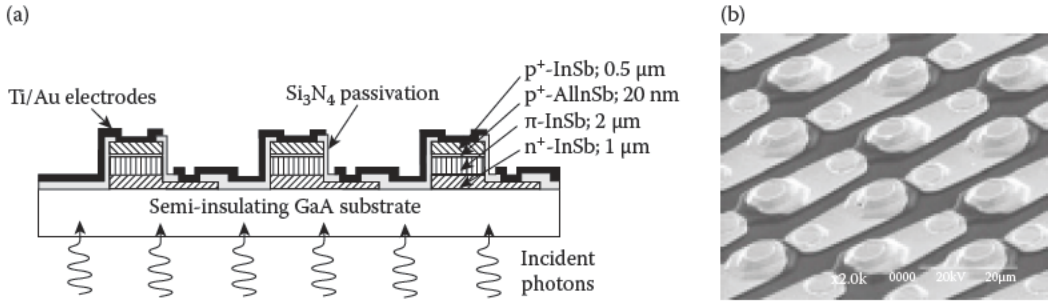
reverse bias, making BLIP operation possible. The quantum efficiency in InSb photodiodes optimized for this temperature range remains unaffected up to 160 K (see Figure 13.26 [108]). Process modifications such as increases in doping density allow responsivity to remain unchanged by increasing temperature.

Some of the design constraints associated with bulk devices with implanted or diffusion junctions can be relaxed using epitaxial methods. Epitaxial, BSI InSb photodiodes have been grown on Te-doped InSb substrates. Degenerate n-type doping of the substrates allows them to be made transparent through the Burstein-Moss effect. A doping of 2×10^{18} cm^{-3} is sufficient to obtain transparency at 80 K over the majority of the 3–5 μm wavelength range [148]. Free carrier absorption requires that the substrates are polished back to a thickness of 100 μm. However, to obtain high quantum efficiency the substrate should be thinned to a value of the order of 10 μm, as in the case for bulk devices. The p$^+$ and n$^+$ regions are doped to 3×10^{18} cm^{-3} and 2×10^{18} cm^{-3}, respectively, and the active region has an n-type doping of approximately 2×10^{15} cm^{-3}. The thicknesses of the p$^+$, n$^+$, and active regions are 1 μm, 4 μm, and 3 μm, respectively. During array fabrication procedures, the wafers are patterned on a 30 μm pitch using standard lithography, then profiled to mesa shapes by a chemical etch down to the n$^+$ region. The final size is approximately 17 μm at the diode junction.

The InSb photodiodes grown heteroepitaxially on Si and GaAs substrates by MBE have been also reported [20,149–154]. Recently, Kuze et al. [153,154] have developed a novel microchip-sized InSb photodiode sensor, on semi-insulating GaAs(100) substrate, operating at detection. The sensor consists of 910 photodiodes connected in series (see Figure 13.27). Each photodiode consists of MBE grown 1 μm thick n$^+$-InSb layer, followed by a 2 μm thick π-InSb absorber layer. To reduce the diffusion of photoexcited electrons, a 20 nm thick p$^+$-Al$_{0.17}$In$_{0.83}$Sb barrier layer was grown on the π-InSb layer. Finally, a 0.5 μm thick π-InSb layer was grown as the top contact. As the n- and p-type dopants Sn and Zn were used, respectively, with concentrations of 7×10^{18} cm^{-3} for the n$^+$-layer, 6×10^{16} cm^{-3} for the π layer, and 2×10^{18} cm^{-3} for the p$^+$ layer. To insulate mesa structures, a 300 nm thick plasma CVD passivation Si$_3$N$_4$ layer was deposited. Finally, after Ti/Au lift-off metallization, a 300 nm thick SiO$_2$ passivation also grown by plasma CVD was made. The length of a single InSb photodiode was 20 μm. The final external dimensions of photovoltaic infrared sensor were $1\,9 \times 2.7 \times 0.4$ mm^2. The sensitivity and the noise equivalent difference temperature were 127 μV/K and 1 mK/Hz$^{1/2}$, respectively.

13.3.4 InAs Photodiodes

InAs detectors have been made to operate in the photoconductive, photovoltaic, and PEM modes. Recently however, wider applications (laser warning receivers, process control monitors, temperature sensors, pulsed laser monitors, and infrared spectroscopy) have found InAs photodiodes operated at near room temperature. The photodiodes are mainly fabricated by ion implantation [112,123,124] and the diffusion method [100,102].

(a)

Ti/Au electrodes　　　Si₃N₄ passivation

p⁺-InSb; 0.5 μm
p⁺-AllnSb; 20 nm
π-InSb; 2 μm
n⁺-InSb; 1 μm

Semi-insulating GaA substrate

Incident photons

(b)

Figure 13.27 InSb photovoltaic infrared sensor: (a) schematic structure of multiple photodiodes connected in series, and (b) SEM photograph. (From Camargo, E. G., Ueno, K., Morishita, T., Sato, M., Endo, H., Kurihara, M., Ishibashi, K., and Kuze, M., *IEEE Sensors Journal*, 7, 1335–39, 2007. With permission.)
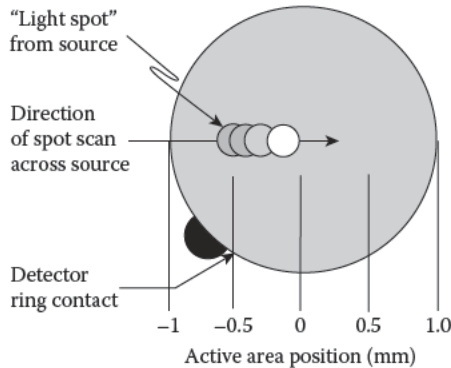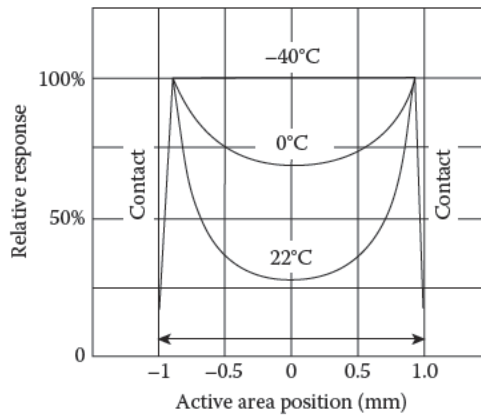

Figure 13.28 InAs photodiodes: (a) response variation across 2 mm active area of InAs photodiodes (After product brochure of Judson Inc., http://www.judsontechnologies.com).

The diode sensitivity, speed of response, impedance, and peak wavelength can be optimized by operation at the proper temperature. At room temperature the shunt resistance of InAs photodiode is comparable with series resistance, which effects the response of photodiodes (see Figure 13.28). This effect is less pronounced in small area detectors, which have higher shunt resistance and less surface area. The effect is also reduced or eliminated by cooling the diode, thereby increasing the junction resistance. InAs photodiodes are sensitive in the 1–3.6 μm wavelength range. A typical range of detectivity for InAs photodiodes is shown in Figure 13.29.

Kuan et al. have presented high performance InAs photodiodes grown by MBE [135,155]. The diode structure was grown on the (100) n-type InAs wafers. After removing the surface oxides
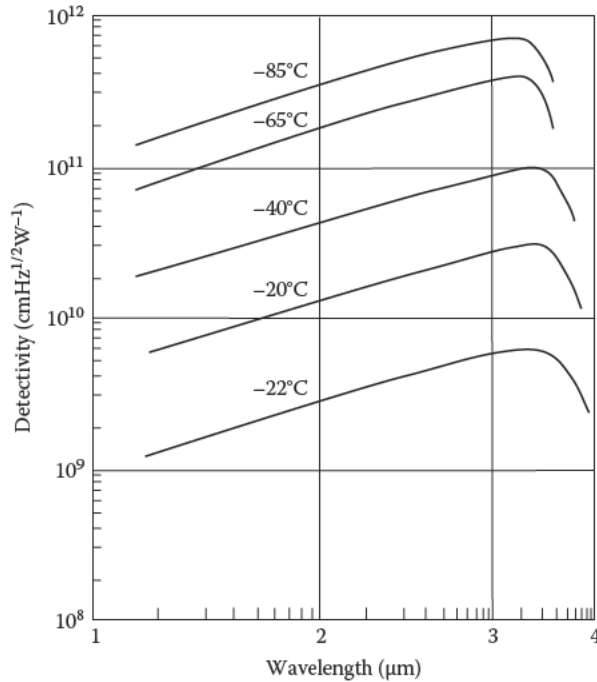
Figure 13.29 Detectivity versus wavelength for InAs photodiodes at different temperatures (After product brochure of Judson Inc., http://www.judsontechnologies.com).
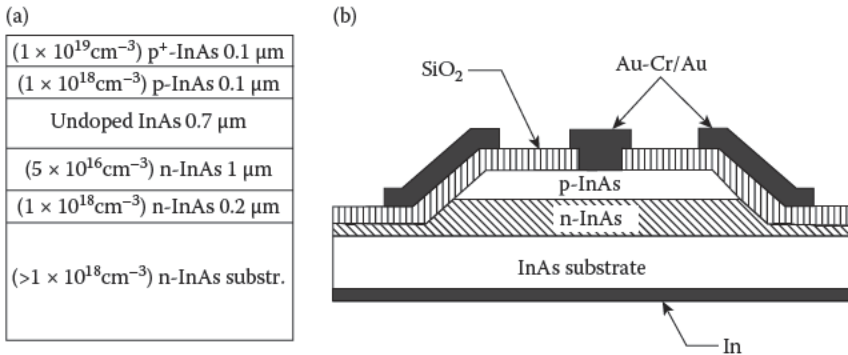
Figure 13.30 InAs gate-controlled photodiode: (a) the schematic diagram, and (b) the device structure. (From Lin, R. M., Tang, S. F., Lee, S. C., Kuan, C. H., Chen, G. S., Sun, T. P., and Wu, J. C., *IEEE Transactions on Electron Devices*, 44, 209–13, 1997. With permission.)

(by slowly heating to 500°C), the InAs epilayers were grown at 500°C under optimized growth conditions. The p-i-n photodiode structure consisted of a 0.2 μm thick n-type buffer layer (Si-doped to 1×10^{18} cm^{-3}), followed by a 1 μm thick n-type InAs active layer (Si-doped to 5×10^{16} cm^{-3}). Then a 0.72 μm thick undoped InAs layer was grown, followed by a 0.1 μm thick p-type InAs layer (Be-doped to 1×10^{18} cm^{-3}), and finally a 0.1 μm thick InAs contact layer (exponentially graded doping from 1×10^{8} cm^{-3} to 1×10^{19} cm^{-3}) was deposited. The same structure was also grown except for the undoped InAs layer for p-n diode. The schematic diagram and device structure of the InAs gate-controlled photodiode are shown in Figure 13.30 [155].

Before fabricating unpassivated and passivated InAs diodes, a special chemical treatment and two-step photolithographic procedures were used [155]. In the case of gate-controlled photodiodes, the epilayers were first mesa etched into circular dots measured 200 μm in diameter and then the
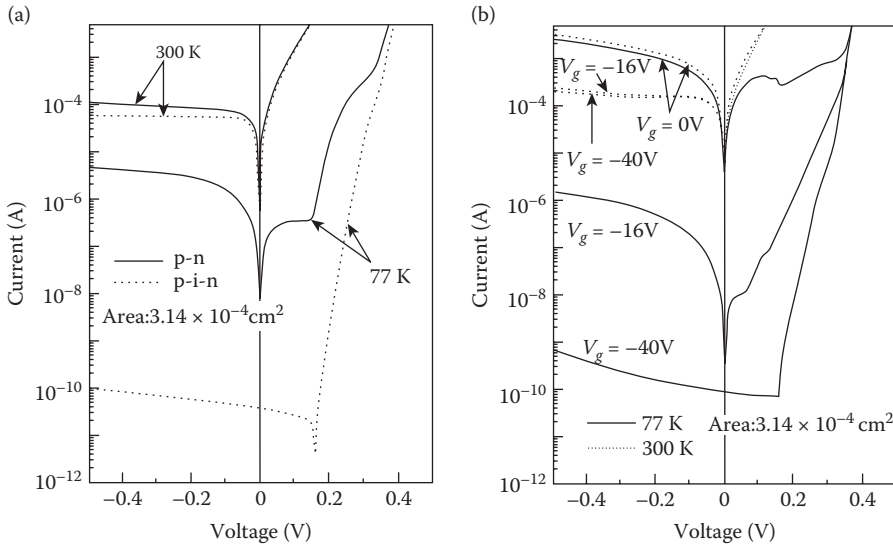
Figure 13.31 The 77 K and room temperature I-V characteristics of the (a) unpassivated, and (b) gate-controlled InAs p-i-n and p-n photodiodes. The gate biases ($V_g = 0$, –16, and –40V) are marked in (b). (From Lin, R. M., Tang, S. F., Lee, S. C., Kuan, C. H., Chen, G. S., Sun, T. P., and Wu, J. C., *IEEE Transactions on Electron Devices,* 44, 209–13, 1997. With permission.)

photo-CVD technique was applied to deposit 300 nm thick SiO_2. A second photolithographic step was used to remove the SiO_2 from the defined area of $10 \times 4\ \mu m^2$ on the p-type layer in order to make electrical contacts. A double layer of 100 nm thick Au-Be and 300 nm thick Au was evaporated sequentially and lifted off to form a p-type ohmic contact. A third photolithographic step was used to define the pad with a dot having a 40 μm diameter and the gate electrode that covered the junction perimeter. Then a double layer of 12 nm of Cr and 300 nm of Au were evaporated and lifted off.

Analysis and comparison of the dark current characteristics between InAs p-n and p-i-n diodes at the temperature range from 30 to 300 K carried out by Kuan and colleagues [135] indicated that incorporation of a thick i-layer (i.e., 720 nm) is the key to success of the detector. The advantage of the p-i-n structure is not only to cut down the tunneling current but also to increase the uniformity.

Figure 13.31a shows the typical 77 K and room temperature I-V characteristics of unpassivated p-i-n and p-n photodiodes, respectively [155]. At 77 K, the dark current of unpassivated p-i-n photodiode is disturbed by the background thermal radiation, proof of which is the existence of a photovoltage. We can also see that the reverse dark current of unpassivated photodiode depends on the diode reverse bias both at 77 K and 300 K indicating the existence of a shunt leakage current. Figure 13.31b shows the typical 77 and 300 K I-V characteristics of gate-controlled p-i-n photodiodes under different gate bias at 0, –16, and –40 V. The strong dependence of the diode reverse dark current on the gate voltage indicates that the reverse leakage current is flowing through the surface region. When the gate bias V_g approaches –40 V, the reverse dark current becomes nearly independent of reverse biases, which indicates that the diode is leakage free. It is obvious that the I-V characteristics of unpassivated p-i-n photodiode is similar to and even better than the p-i-n gate-controlled photodiode under gate bias $V_g = -40$ V. This indicates that passivation of InAs p-i-n photodiode degrades the device performance. The unpassivated p-i-n photodiode exhibits R_oA product of 8.1 Ωcm^2 at room temperature and 1.3 $M\Omega cm^2$ at 77 K. When illuminated under a 500 K blackbody source, the photodiode detectivity limited by Johnson noise is 1.2×10^{10} $cmHz^{1/2}W^{-1}$ at room temperature and 8.1×10^{11} $cmHz^{1/2}W^{-1}$ at 77 K.

Alternative substrates in fabrication InAs photodiodes have also been used. Dobbelaere et al. have produced InAs photodiodes grown on GaAs and GaAs-coated Si by MBE [156]. This technique is suitable for fabrication of monolithic near-infrared imagers where a combination of detection with silicon readout electronics is possible.

(a)

(b)
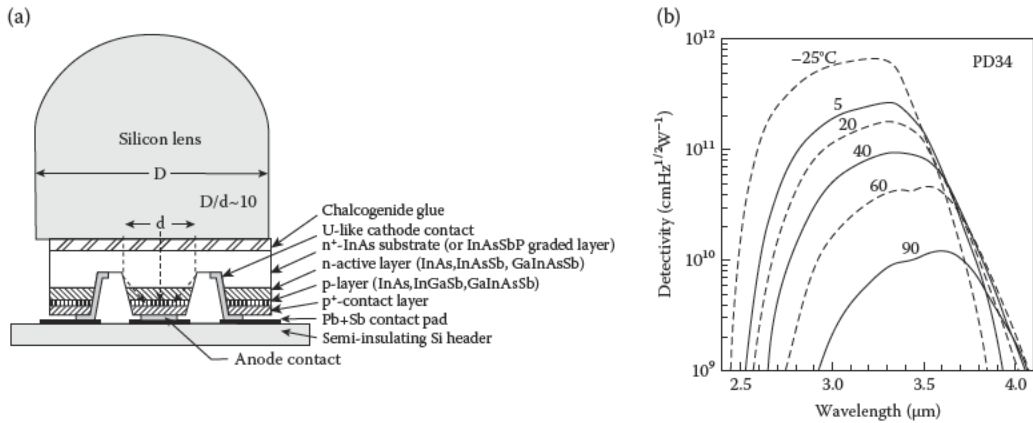
Figure 13.32 InAs heterostructure immersion photodiode: (a) construction of the immersion photodiode, and (b) detectivity spectral at near-room temperatures. (From Remennyy, M. A., Matveev, B. A., Zotova, N. V., Karandashev, S. A., Stus, N. M., and Ilinskaya, N. D., "InAs and InAs(Sb)(P) (3–5 μm) Immersion Lens Photodiodes for Potable Optic Sensors," *Proceedings of SPIE* 6585, 658504, 2007. With permission.)

Recently, the research group at the Ioffe Physico-Technical Institute (St. Petersburg, Russia) has developed InAs immersion-lens photodiodes operated at near-room temperatures [132]. InAs heterostructure photodiodes (see Figure 13.32a) were LPE grown onto n^+-InAs transparent substrates (due to the Burstein–Moss effect) and consisted of ~3 μm thick n-InAs layers and ~3 μm thick p-InAs$_{1-x-y}$Sb$_x$P$_y$ cladding layers lattice matched with InAs substrate ($y \sim 2.2x$). Due to an energy step at the n^+-InAs/n-InAs interface, a beneficial hole confinement for the photodiode operation is expected. Flip-chip mesa devices with the diameter of 280 μm were processed by a multistage wet photolithography process. A cathode as well as anode contacts were formed by sputtering of Cr, Ni, Au(Te), and Cr, Ni, and Au(Zn) metals followed by an electrochemical deposition of a 1–2 μm thick gold layer. Next the substrate was thinned down to 150 μm and chips were soldered onto silicon submounts with Pb–Sn contact pads. Finally, the 3.5 mm wide silicon lens was attached to the substrate side of a chip by a chalcogenide glass with high refractive index ($n = 2.4$). It is obvious that the field of view of immersion photodiodes is considerable lower than for uncoated device (decreased down to 15°).

Figure 13.32b shows the detectivity spectra of InAs heterostructure immersion photodiode. Superior detectivity of these photodiodes (for comparison see Figure 13.29) reflects improvements associated with board mirror contact, asymmetric doping, immersion effect, and radiation collection by inclined mesa walls. The narrow spectral responses are a result of filtering in the substrate and intermediate layers. Peak wavelengths shift to long wavelengths as temperature is increased due to bandgap narrowing at higher temperatures. However, the short wavelength spectra are more sensitive to temperature than the long wavelength ones probably due to progressively poor transparency of n^+-InAs near the absorption edge at elevated temperatures due to elimination of the conduction band electron degeneration [132].

13.3.5 InSb Nonequilibrium Photodiodes

The first nonequilibrium InSb detectors had a p^+-π-n^+ structure, where π represents low doped p-type material that is intrinsic at the temperature of operation [18]. An accurate analysis of the source of current in the diode at room temperature indicates the predominant contribution of Auger seven generation in the p^+ material. At temperatures below 200 K, the performance of photodiodes is determined by Shockley–Read generation in the π region (Figure 13.33). Davies and White investigated the residual currents in Auger suppressed photodiodes [157]. They find that removing electrons from the active region alters the occupancy of the traps leading to an increased generation rate from the Shockley–Read traps in the active region.

Next it was shown that a thin strained layer of InAlSb between the p^+ and π regions produces a barrier in the conduction band that substantially reduces the diffusion of electrons from the p^+ layer to the π region leading to an improvement in room temperature performance [19,158]. This type of p^+-P^+-π-n^+ InSb/In$_{1-x}$Al$_x$Sb structure shown schematically in Figure 13.34 was fabricated
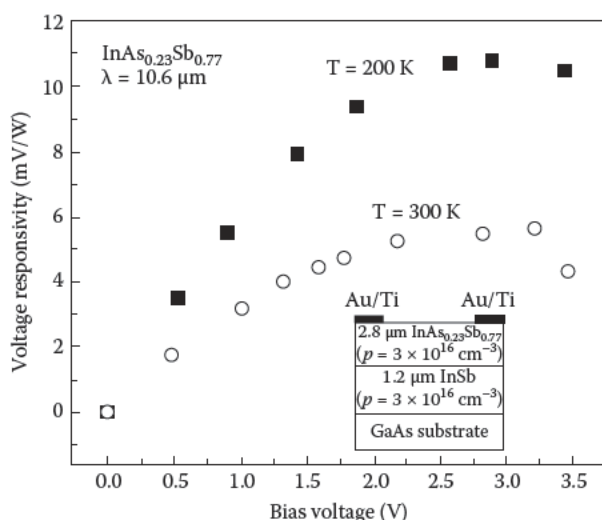
Figure 13.39 Voltage-dependent responsivity of the InAs$_{0.23}$Sb$_{0.77}$ photoconductor at 10.6 µm. (From Kim, J. D., Wu, D., Wojkowski, J., Piotrowski, J., Xu, J., and Razeghi, M., *Applied Physics Letters*, 68, 99–101, 1996. With permission.)

corresponds to the values of 5.8 mV/W at 300 K and 10.8 mV/W at 200 K, respectively. The corresponding Johnson-noise limited detectivity was estimated to be $\approx 3.27 \times 10^7$ cmHz$^{1/2}$W^{-1} at 300 K. This is below the theoretical limit ($\approx 1.5 \times 10^8$ cmHz$^{1/2}$W^{-1}) set by Auger g–r process.

13.4.1.2 InAsSb Photodiodes

The main effort in InAsSb detector technology has been shifted to the development of photodiodes as useful devices for the second-generation thermal-imaging systems and the next generation very low loss fiber communication systems [17,37,45]. During the last three decades high-quality InAsSb photodiodes for the 3–5 µm spectral region have been developed [132,176–197]. The long wavelength limit of InAs$_{1-x}$Sb$_x$ detectors has been tuned compositionally from 3.1 µm ($x = 0.0$) to 7.0 µm ($x \approx 0.6$). Potentially the material is capable of operating at the longest cutoff wavelength (≈ 9.0 µm at 77 K) of the entire III–V alloy family [17,37]. To realize IR detectors in all potentially capable operating regions, lattice-matched substrates are necessary. This problem seems to be resolved by using Ga$_{1-x}$In$_x$Sb substrates. In this case the lattice parameter can be tuned between 6.095 Å (GaSb) and 6.479 Å (InSb). Several research groups have succeeded in growing GaInSb single crystals [148,198–200]. One composition worth noting is Ga$_{0.38}$In$_{0.62}$Sb that is lattice matched to InAs$_{0.35}$Sb$_{0.65}$, which has a bandgap minimum, corresponding to ~12 µm at room temperature.

A variety of InAsSb photodiode configurations have been proposed including mesa and planar, n-p, n-p$^+$, p$^+$-n, and p-i-n structures. The techniques used to form p-n junctions have included diffusion of Zn, Be ion implantation, and the creation of p-type layers on n-type material by LPE, MBE, and MOCVD. The photodiode technology relies essentially on n-type material with concentrations generally about 10^{16} cm^{-3}. A summary of works for the fabrication of InAsSb photodiodes is given in Table 13.2.

At first, InAs$_{0.85}$Sb$_{0.15}$ photodiodes grown by a step-graded LPE technique on InAs substrates were reported [176]. A series of InAsSb compositionally step-graded buffer layers were introduced between active layers and the InAs substrate to relieve strain caused by lattice mismatch. The device was operated in the BSI mode. In this case, photons enter through the InAs substrate and through sufficiently thick buffer layers and on a filter layer to absorb most incoming photons with energy greater than the energy bandgap of the filter layer. The cutoff wavelength is mainly determined by the energy bandgap of the active layer and spectral characteristics can be controlled by the Sb composition of the filter layer and active layer. The carrier concentration across the junction is $\approx 10^{15}$ cm^{-3} for n-type and $\approx 10^{16}$ cm^{-3} for p-type. Mesa photodiodes fabricated in this way exhibit excellent characteristics as narrow-band BSI infrared detectors. Half-widths of spectral response

Table 13.2: Performance of InAs$_{1-x}$Sb$_x$ Photodiodes

Material	Fabrication	T (K)	R_oA (Ωcm²)	λ_p (μm)	η (%)	D* (cmHz$^{1/2}$W^{-1})	Comments	Refs.
n-p⁺ InAs$_{0.85}$Sb$_{0.15}$	mesa, step-graded LPE (n ≈ 10¹⁵ cm⁻³)	77	2×10⁷	4.2	60		InAs substrate, back side illuminated	176
n-p InAs$_{0.86}$Sb$_{0.14}$	mesa, LPE, (n ≈ p ≈ 10¹⁶ cm⁻³)	77	10⁹	4.2	65		GaSb substrate, back side illuminated	178
n-p⁺ InAs$_{0.85}$Sb$_{0.15}$	planar, LPE, (n ≈ 10¹⁶ cm⁻³), Be implantation	77	10⁷		80	4×10¹¹	GaSb substrate, CVD SiO₂ as a implantation mask, back side illuminated, 10¹⁵ ph/cm²s	177
n-p InAs$_{0.85}$Sb$_{0.15}$	mesa, LPE, (n ≈ p ≈ 10¹⁷ cm⁻³)	77 / 200		3.5 / 3.0	40 / 40	1.5×10¹¹ / 2.0×10¹⁰	InAs substrate / 2π FOV	180
n-i-p InAs$_{0.85}$Sb$_{0.15}$	mesa, MBE n ≈ p ≈ (2–20)×10¹⁶cm⁻³, i ≈ 3×10¹⁵ cm⁻³	77 / 77 / 77	49 / 25 / 1.9	3.5 / 3.5 / 3.5		1.5×10¹¹ / 1.6×10¹¹ / 4.5×10¹⁰	InAs substrate / GaAs substrate / Si substrate	182
n-p InAs$_{0.88}$Sb$_{0.12}$	mesa, LPE	77 / 200	2	3.8 / 4.3		3.0×10¹¹ / 5×10⁹	InAs substrate, front side illumination	184
P-GaSb/i-InAs$_{0.91}$Sb$_{0.09}$/N-GaSb	mesa, MBE i(1 μm) ≈ 10¹⁶ cm⁻³	250		3.39		2.5×10¹⁰	N-GaSb substrate, double heterojunction	195
n-InAs$_{0.91}$Sb$_{0.09}$/N-GaSb	mesa, MOCVD n(2.65 μm) ≈ 1.06×10¹⁶ cm⁻³ N ≈ 1.1×10¹⁸ cm⁻³	300 / 180	2–3 / 180	≈ 4		4.9×10⁹ / 1.3×10¹⁰	N-GaSb substrate, front side illumination, izotype heterojunction, detectivity measured at reverse bias, bias tuning two-color detection	197
p⁺-InAs$_{0.91}$Sb$_{0.09}$/P⁺-InAlAsSb/ n-InAs$_{0.91}$Sb$_{0.09}$/p⁺-InAs$_{0.91}$Sb$_{0.09}$	mesa, MBE n(2 μm) ≈ 2×10¹⁶ cm⁻³	300 / 230	0.19 / 10.9	4 / 3.7		2.6×10⁹ / 4.2×10¹⁰	P-GaSb substrate, front side illumination, 2 μm thick In$_{0.88}$Al$_{0.12}$As$_{0.80}$Sb$_{0.20}$ barrier nearly matches with active layer leads to efficient transport of photogenerated holes	193
N⁺-InAs/n-InAsSb/P-InAsSbP	mesa, LPE N⁺ ≈ 10¹⁸ cm⁻³ n(3–8 μm) undoped, ≈ 10¹⁶ cm⁻³	300	2×10⁻²	4.2		2×10¹⁰	N⁺-InAs substrate, back side illumination, optical immersion (Si lens)	132

Structure	Details	T (K)			D^*	Comments	Ref.
N$^+$-InAs/N$^+$-InAs$_{0.55}$Sb$_{0.15}$P$_{0.30}$/n-InAs$_{0.89}$Sb$_{0.11}$/P-InAs$_{0.55}$Sb$_{0.15}$P$_{0.30}$	mesa, LPE n(5 μm) undoped active region sandwiched between two (3 μm thick) InAsSbP cladding layers	300		4.5	1.26×10^9	N$^+$-InAs substrate, front side illumination	185
P$^+$-AlGaAsSb/AlInAsSb/n-InAs$_{0.91}$Sb$_{0.09}$/N$^+$-GaSb	mesa, MBE n(1.6 μm) $\approx 3 \times 10^{16}$ cm^{-3} undoped active region, alkali sulfur passivation	300	3	4.3	1×10^{10}	N-GaSb substrate, AlGaAsSb used as a transparent window, AlInAsSb reduces the hole confinement at the InAsSb/AlGaAsSb heterointerface, front side illumination	191
p$^+$-InSb/π-InAs$_{0.15}$Sb$_{0.85}$/n$^+$-InSb	mesa, MOCVD n$^+$(2 μm) $\approx 3 \times 10^{18}$ cm^{-3} π(3 μm) $\approx 3.6 \times 10^{16}$ cm^{-3} p$^+$(0.5 μm)) $\approx 3 \times 10^{18}$ cm^{-3}	300	2×10^{-4}	≈ 8	1.5×10^8	GaAs substrate, back side illuminated $\lambda_c \approx 13$ μm	183
p$^+$-InSb/π-InAs$_{0.15}$Sb$_{0.85}$/n$^+$-AlInSb	mesa, MBE n$^+$(2 μm) $\approx 3 \times 10^{18}$ cm^{-3} π(3 μm) $\approx 3.6 \times 10^{16}$ cm^{-3} p$^+$(0.5 μm) $\approx 3 \times 10^{18}$ cm^{-3}	300	0.11	6	$\approx 3 \times 10^8$	GaAs substrate, back side illuminated,incorporating of AlInSb buffer layer blocks carriers from the highly dislocation interface	20
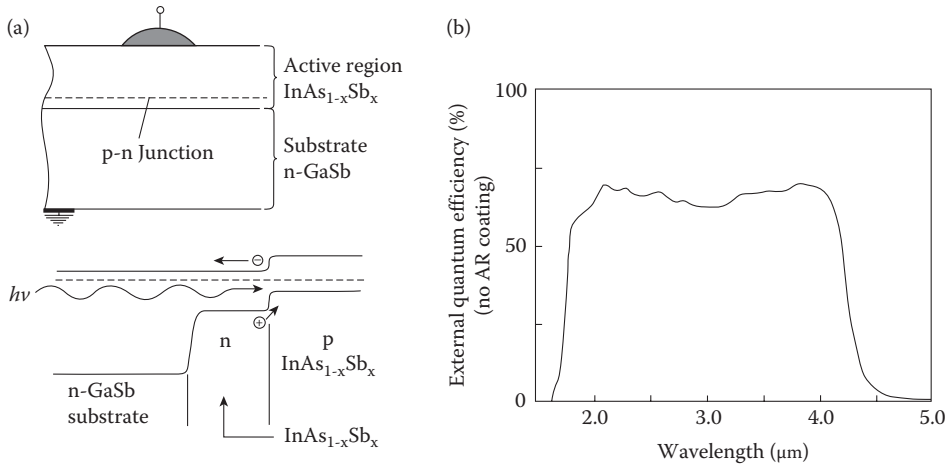
Figure 13.40 Back side illuminated InAs$_{0.86}$Sb$_{0.14}$/GaSb photodiode: (a) device structure and energy band diagram of the structure, and (b) spectral response at 77 K. (From Bubulac, L. O., Andrews, A. M., Gertner, E. R., and Cheung, D. T., *Applied Physics Letters*, 36, 734–36, 1980. With permission.)

as narrow as 176 nm at 77 K with peak internal quantum efficiency of 70% has been achieved. The zero-bias resistance area R_oA products are in the 10^5 Ωcm^2 range, with the best ones achieving 2×10^7 Ωcm^2.

The best performances of InAsSb photodiodes have been obtained when lattice-matched InAs$_{1-x}$Sb$_x$/GaSb ($0.09 \leq x \leq 0.15$) device structures were used [178]. Lattice mismatch up to 0.25% for the InAs$_{0.86}$Sb$_{0.14}$ epitaxial layer can be accommodated in terms of low etch-pit density ($\approx 10^4$ cm^{-2}). The structure of a BSI InAs$_{1-x}$Sb$_x$/GaSb photodiode is shown in Figure 13.40a [178]. The photons enter through the GaSb transparent substrate and reach the InAs$_{1-x}$Sb$_x$ active layer where they are absorbed. The GaSb substrate determines the short-wavelength cut-on value, which is 1.7 μm at 77 K; instead the active region establishes the long-wavelength cutoff value (see Figure 13.40b). The p-n junctions were obtained as homojunctions using the LPE technique. The carrier concentrations, both in the undoped n-type layer and in the Zn doped p-type layer, were approximately 10^{16} cm^{-3}. The high quality of InAs$_{0.86}$Sb$_{0.14}$ photodiodes was demonstrated by a high R_oA product in excess of 10^9 Ωcm^2 at 77 K.

High performance InAs$_{0.89}$Sb$_{0.11}$ photodiodes have also been obtained by Be ion implantation [177]. The as-grown LPE layers on (100) GaSb substrates were n-type with a typical carrier concentration of 10^{16} cm^{-3}. The implantation mask was formed by 100 nm of CVD SiO$_2$ deposited at 200ºC and next covered with about 5 μm of photoresist or about 700 nm of aluminum. The Be ion implantation was performed using a 100 keV beam and a total dose of 5×10^{15} cm^{-2}. Following the implantation, annealing was carried out at 550ºC for about 1 hr. The EBIC analysis of the InAs$_{0.89}$Sb$_{0.11}$ planar junction and *C-V* data confirmed the junction formation by the thermodiffusion mechanism.

Attempts to MBE grow InAs$_{0.85}$Sb$_{0.15}$ p-i-n junctions on lattice mismatched substrates—InAs (lattice mismatch 1%), GaAs (8.4%), and Si (12.8%)—have not given good results [182]. The performance of these photodiodes was inferior in comparison with the ones fabricated using LPE. Their R_oA product was almost three orders lower than photodiodes obtained by LPE [176–178]—below 50 Ωcm^2 at 77 K for diodes on InAs. The diodes exhibited significantly larger reverse leakage currents. The presence of defects reduces the carrier lifetime so that the g–r currents become increasingly important. To decrease the influence of misfit dislocations, different procedures were followed in deposition of interface regions, which are described exactly by Dobbelaere and colleagues [201,202].

Rogalski has performed an analysis of a resistance-area product (R_oA) of n-p$^+$ abrupt InAs$_{0.85}$Sb$_{0.15}$ junctions at 77 K [45]. The dependence of the ultimate values of the R$_o$A product on the concentrations of dopants for abrupt n-p$^+$ InAs$_{0.85}$Sb$_{0.15}$ photodiodes at 77 K is shown in Figure 13.41a. We can see that the R_oA product is determined by the g–r current of the junction depletion layer. The characteristic lifetime in the depletion region τ_o determined from
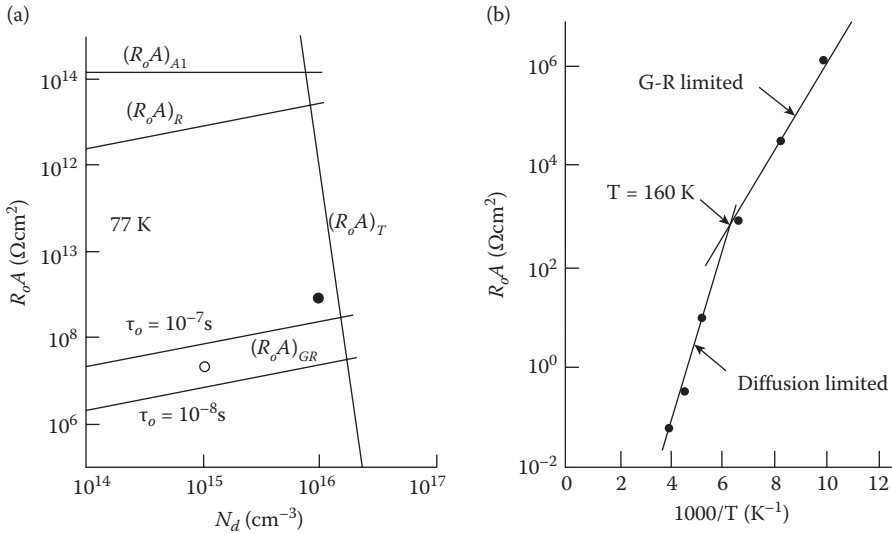
Figure 13.41 R_oA product of InAs$_{1-x}$Sb$_x$ photodiodes: (a) dependence on the doping concentration for n-p$^+$ abrupt InAs$_{0.85}$Sb$_{0.15}$ junctions at 77 K, the experimental values are taken from Cheung [176] (o) and Bubulac [178] (•). (From Rogalski, A., *Progress in Quantum Electronics*, 13, 191–231, 1989.) (b) Dependence on the temperature for a typical planar Be implanted InAs$_{0.89}$Sb$_{0.11}$ photodiode. (From Bubulac, L. O., Barrowcliff, E. E., Tennant, W. E., Pasko, J. P., Williams, G., Andrews, A. M., Cheung, D. T., and Gertner, E. R., *Institute of Physics Conference Series No. 45*, 519–29, 1979. With permission.)

the theoretical fit to the g–r model is found to be 0.03–0.5 μs. In the best photodiodes it was determined to be 0.55 μs [178]. The theoretical estimates yield for the radiative $(R_oA)_R$ and Auger recombination $(R_oA)_{A1}$ values of the R_oA product of several orders of magnitude larger. Tunneling current produces an abrupt lowering of R_oA at a concentration a little above 10^{16} cm^{-3}. To obtain a possibly high value of the zero-bias resistance of the junction, the technological process of photodiode preparation should be conducted so that the concentration of dopants is slightly below 10^{16} cm^{-3}.

Each of the current components of the p-n junction has its own individual relationship to voltage and temperature and can be associated with either the bulk or the surface. In Figure 13.41b the R_oA product against $1/T$ for Be ion implantation InAs$_{0.89}$Sb$_{0.11}$ junction is plotted [177]. In a semilog scale representation R_oA varies linearly for the g–r and diffusion model, as $1/n_i$ and $1/n_i^2$, respectively. In the temperature range above 160 K, the R_oA product follows the diffusion model, whereas in the temperature range $80 \le T \le 160$ K, R_oA fits a g–r model. At temperatures below 80 K the R_oA product is limited by surface effects. Therefore the operation of planar Be-implanted photodiodes is bulk-limited above 80 K.

Attempts to fabricate p-n junction formation in the miscibility range of InAs$_{1-x}$Sb$_x$ ternary alloy over the composition range $0.4 < x < 0.7$ using MOCVD have not given positive results [203]. The p$^+$-n junctions were formed by Zn diffusion into the undoped n-type epitaxial layer with carrier concentration in the range of 10^{16} cm^{-3}. The forward and the reverse characteristics were affected by the g–r current of the depletion region and by surface leakage current. It is believed that recombination centers in the depletion layer were caused by diffusion-induced damages and by lattice mismatch dislocations between the InAs$_{0.60}$Sb$_{0.40}$ epilayer and the InSb substrate.

Generally, the low-temperature homojunction devices suffer from Shockley–Read generation current and the activation energy decreases to about half the bandgap energy [45,188]. At high temperatures, where the diffusion current mechanism is dominant, these homojunction devices exhibit a large dark current and small R_oA product, below 10^{-2} Ωcm^2, which leads to relatively low detectivity.

In order to improve device performance (lower dark current and higher detectivity) several groups have developed P-i-N heterostructure devices of an unintentionally doped InAsSb active layer sandwiched between P and N layers of larger bandgap materials. As is shown in Section 3.2,
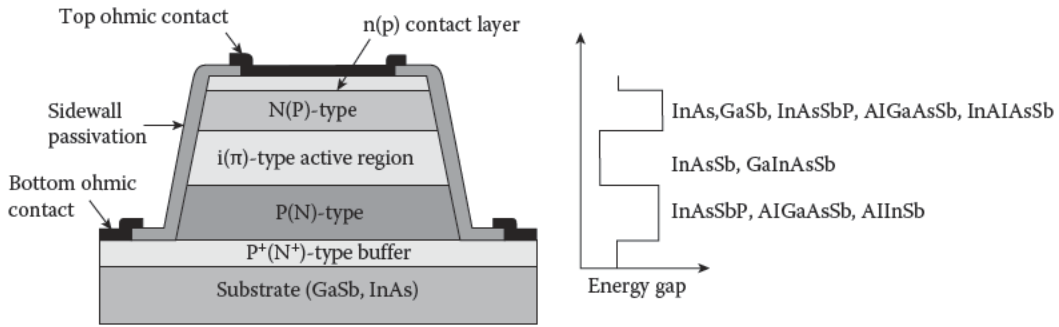
Figure 13.42 Schematic band diagram of the N-i-P double heterostructure antimonide based III-V photodiodes. Different combinations of active and cladding layers are also shown.

the lower minority carrier concentration in the high bandgap layers resulted in a lower diffusion dark and higher R_oA product and detectivity. Figure 13.42 shows a schematic band diagram of the N-i-P double heterostructure antimonide based III-V photodiodes together with the different combinations of active and cladding layers in the device structure. In dependence on contact configurations and transparency of substrates, both back side and front side illumination can be used. Usually p-type GaSb and n-type InAs are used. Despite the relatively low absorption coefficients, substrates required thinning to small thicknesses, even less than 25 µm. InAs is fragile and many fabrication processes are not possible. This obstacle can be overcame by using heavily doped n^+-InAs substrates where strong degeneracy of the electrons in the conduction band occurs at relatively low electron concentration ($> 10^{17}$ cm^{-3}). For example, the Burstein-Moss shift in heavily doped n^+-InAs ($n = 6 \times 10^{18}$ cm^{-3}) makes the corresponding substrates transparent to the 3.3 µm [132].

Table 13.2 has short information about InAsSb heterostructure photodiode fabrications and their performance. Considerable progress in the development of LPE antimonide based heterostructure photodiodes has been achieved at the Ioffe Physical-Technical Institute in St. Petersburg, Russia. The knowledge about a thermodynamic data of coexisting phases in LPE process has been achieved by the development of the original method based on excess thermodynamic functions and linear combinations of chemical potentials [204]. In this way the phase diagrams for the Ga-In-As-Sb, In-As-Sb-P, Ga-In-As-Pb, and Ga-Al-As-Sb systems have been calculated. An idea was introduced using Pb as a neutral solvent during LPE growth of both GaSb and InAs layers and caused considerable decrease of the structural defect concentration in GaSb solid solutions from 2.8×10^{17} up to 2×10^{15} cm^{-3} [205]. Moreover, the use of Pb introduces undoped GaInAsSb solid solution with low concentration of defects and impurities and with high carrier mobility [206].

The LPE InAsSb heterostructure photodiodes were grown on heavily doped (111) n^+-InAs(Sn) substrates with electron concentration of 10^{18} cm^{-3} and the density of each pits of 10^4–10^5 cm^{-2}. They consisted of 5 µm thick Zn doped p-InAsSbP [$E_g = 375$ meV, $p = (2$–$5) \times 10^{17}$ cm^{-3}] deposited on 3–8 µm thick undoped InAsSb active layers. Figure 13.43a shows the near room temperature detectivity variation of InAsSb photodiodes with immersion Si lens (see Figure 13.32a) [132]. The short wavelength sharp fall of spectral response is related to InAs substrate transparency.

Also InAsSbP immersion photodiodes, which spectral detectivities are shown in Figure 13.43b, have been fabricated by LPE. However in this case 25–60 µm thick InAsSbP graded bandgap epilayers with low dislocation density (10^4 cm^{-2}) have been grown at 650°C –680°C onto 350µm thick (111) n-InAs substrates with carrier density of 10^{16} cm^{-3}. The wide band part of the InAsSbP at the interface was a transparent for the photons whose energy is close to the narrow bandgap value of the InAsSb(P) [207]. The high energy sensitivity decline in the graded bandgap photodiodes and is related to a diffusion mechanism. The carriers optically created near a broad band InAsSbP surface diffuse into the narrow band part of the diode (estimated diffusion length is 11–15 µm and is shorter than the thickness of the graded bandgap InAsSbP layer).

The first InAsSb-based long wavelength (8–14 µm) photodiode operating at room temperature has been described by Kim et al. [183]. The structure, grown by low-pressure MOCVD, is designed for the operation of back side (GaAs substrate side) illumination. Figure 13.44 shows the voltage responsivity at various temperatures and inside—schematic of device structure [186].
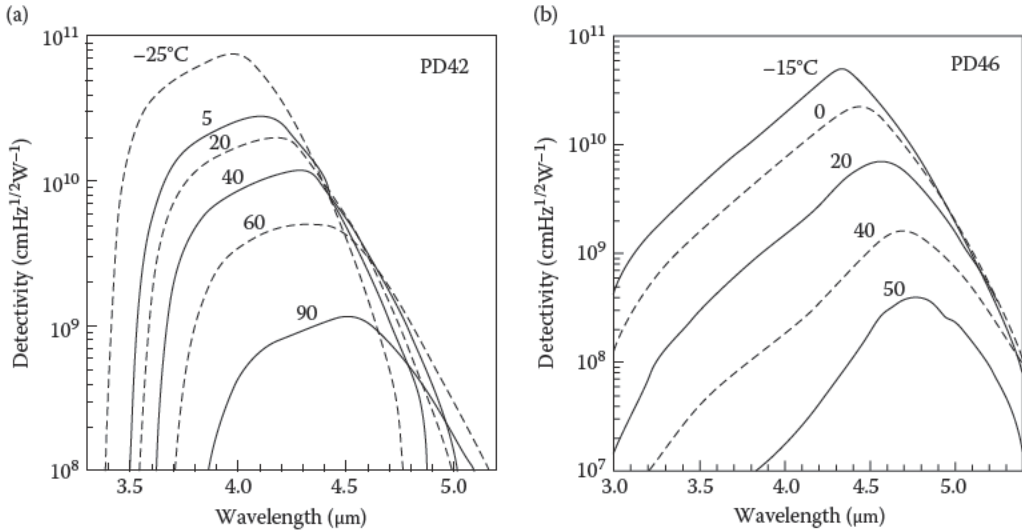
Figure 13.43 Detectivity spectral at (a) near-room temperature InAsSb, and (b) InAsSbP heterostructure photodiodes with optical immersion. (From Remennyy, M. A., Matveev, B. A., Zotova, N. V., Karandashev, S. A., Stus, N. M., and Ilinskaya, N. D., "InAs and InAs(Sb)(P) (3–5 μm) Immersion Lens Photodiodes for Potable Optic Sensors," *Proceedings of SPIE* 6585, 658504, 2007. With permission.)
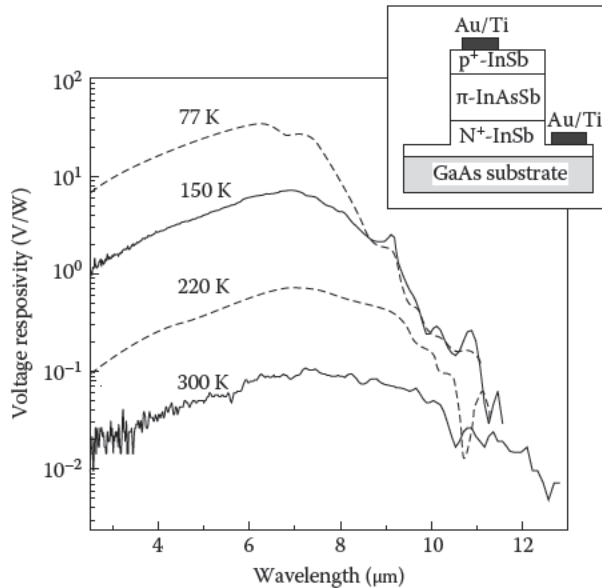
Figure 13.44 Spectral response of the p^+-InSb/π-nAs$_{0.15}$Sb$_{0.85}$/n$^+$-InSb heterojunction device at various temperatures. Inside a schematic device structure is shown. (From Kim, J. D., and Razeghi, M., *Opto-Electronics Review,* 6, 217–30, 1998. With permission.)

Photoresponse up to 13 μm has been obtained at 300 K in an p^+-InSb/π-nAs$_{0.15}$Sb$_{0.85}$/n$^+$-InSb heterojunction device. The peak voltage responsivity is 9.13×10^{-2} V/W at 300 K. At 77 K, it is only 2.85×10^1 V/W, which is much lower than the expected value. Possible reasons are the poor interface properties due to the lattice mismatch between the absorber and contact layers and high dark current due to the high doping level in the active layer. Introducing the AlInSb buffer layer as the
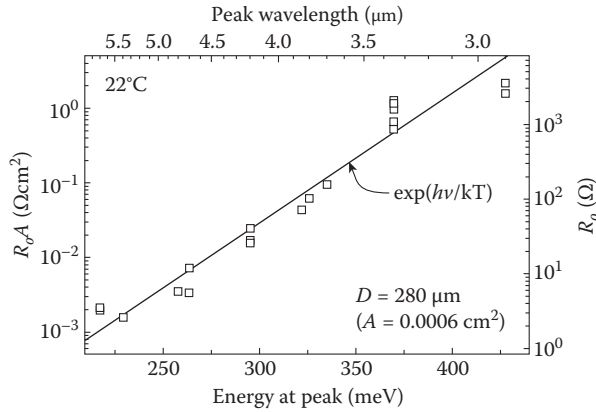
Figure 13.45 R_oA product in series of developed photodiode at room temperature. (From Remennyy, M. A., Matveev, B. A., Zotova, N. V., Karandashev, S. A., Stus, N. M., and Ilinskaya, N. D., "InAs and InAs(Sb)(P) (3–5 μm) Immersion Lens Photodiodes for Potable Optic Sensors," *Proceedings of SPIE* 6585, 658504, 2007. With permission.)

bottom contact layer blocks carriers from the highly dislocated interface resulting in increase of the R_oA product and detectivity [20].

Similar to N-GaInAsSb/n-InAs izotype heterojunction shown in Figure 13.37, also N-GaSb/n-InAsSb rectifying heterostructure has the unique type II broken gap interface [208,209]. A large barrier for electrons is formed in the GaSb side of the interface. Due to differences in electron affinity between two materials, electrons are transferred from the GaSb side to the InAsSb side across the interface. The resultant band banding leads to the formation of a barrier for electrons in the GaSb side and a two-dimensional electron gas in the InAsSb side. The barrier of the N-n interface is comparable to the energy gap of the wider band-gap material (GaSb). Sharabani et al. have shown that N-GaSb/n-In$_{0.91}$As$_{0.09}$Sb heterostructure is a promising material for high operating temperature MWIR detectors [197]. The BLIP temperature was found to be 180 K, and R_oA product of 2.5 and 180 Ωcm^2 were measured at 300 and 180 K, respectively.

### 13.4.2 Photodiodes Based on GaSb-Related Ternary and Quaternary Alloys

GaSb-related ternary and quaternary alloys are well established as materials for developing MWIR photodiodes for near-room temperature operation [127–132,159,165,207,210–212]. At present the research efforts are concentrated mainly on double heterostructure devices; their schematic structure is shown in Figure 13.42. This figure also shows different material systems used in the active and cladding layers.

A recently published paper by Remennyy et al. gives a short overview of GaSb-based photodiode performance [132]. Figure 13.45 summarizes experimental data of zero bias resistivity and R_oA product versus photon energy. An exponential dependence of R_oA product, approximated by $\exp(E_g/kT)$, indicates that the diffusion current determines the transport properties of the heterojunctions at room temperature.

Figure 13.46 presents current responsivities and detectivities in dependence on photon energy for the BSI and the coated photodiodes (with immersion lens, IL) [132]. It is shown that the photodiodes developed at the Ioffe Physical-Technical Institute are superior to the others published in literature. The detectivities shown in Figure 13.46b are higher in comparison with that gathered in Table 13.2 for photodiodes operated in similar conditions. It is expected that higher device performance reflects improvements in device design and fabrication: broad mirror contact and radiation collection by inclined mesa walls.

Narrow-gap III-V semiconductors and their alloys are also promising materials for developing high-speed, low-noise APDs. They have found a number of applications in the 2–5 μm spectral range including: laser-diode spectroscopy, mid-IR fiber optics, laser range-finding, free-space optical links for high frequency communications, and so on.

Many articles have discussed the properties of mid-IR APDs and many of the investigations were made at the Ioffe Institute. Recently Mikhailova and Andreev have published a comprehensive review paper devoted to 2–5-μm APDs [165].
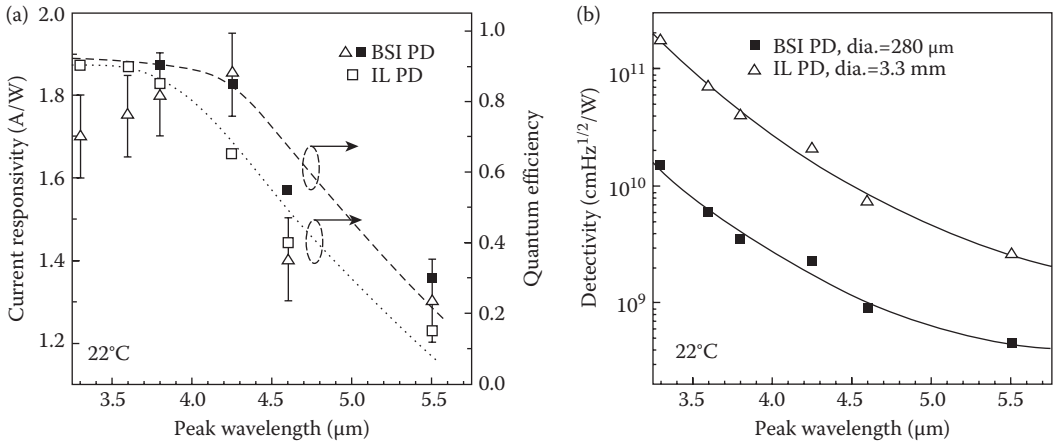
Figure 13.46 (a) Current responsivity and (b) peak detectivity of photodiodes without (back side illuminated, BSI) and with Si lenses (immersion illuminated, IL). (From Remennyy, M. A., Matveev, B. A., Zotova, N. V., Karandashev, S. A., Stus, N. M., and Ilinskaya, N. D., "InAs and InAs(Sb)(P) (3–5 μm) Immersion Lens Photodiodes for Portable Optic Sensors" *Proceedings of SPIE* 6585, 658504, 2007. With permission.)

It is a well-known fact that the excess avalanche noise factor and thus the signal-to-noise ratio of an APD depends on the ratio of electron and hole impact ionization coefficients (α_e and α_h, respectively). To achieve a low noise factor, not only must α_e and α_h be as different as possible, but also the avalanche process must be initiated by the carriers with the higher ionization coefficient. Unlike silicon APDs, it was found that holes dominate the impact ionization process. According to McIntyre's rule, the noise performance of APD can be improved by more than a factor of 10 when the α_h/α_e ionization ratio is increased to 5. For InAs- and GaSb-based alloys, a resonant enhancement of the hole ionization coefficient has been found [165,210,213,214]. This effect is attributed to impact ionization initiated by holes from a split-off valence band: if the spin orbit splitting Δ is equal to the bandgap energy E_g, the threshold energy for hole initiated impact ionization reaches the smallest possible value and the ionization process occurs with zero momentum. This leads to a strong increase of α_h at $\Delta/E_g = 1$.

Figure 13.47 illustrates the electric field dependence of α_e and α_h in the GaInAsSb/GaAlAsSb heterostructure at 230 K [215]. The heterostructure was grown by LPE on < 111 > n-GaSb Te doped substrate with carrier concentration $(5–7) \times 10^{17}$ cm^{-3}. The active region consisted of an unintentionally doped n-type and 2.3 μm thick $Ga_{0.80}In_{0.20}As_{0.17}Sb_{0.83}$ layer ($E_g = 0.54$ eV at 300 K) with carrier density of 2×10^{16} cm^{-3}. The wide-gap "window" layer was 2 μm thick p^+-$Ga_{0.66}Al_{0.34}As_{0.025}Sb_{0.975}$ ($E_g = 1.20$ eV at 300 K) and doped with Ge up to $(1–2) \times 10^{18}$ cm^{-3}. The mesa photodiodes were illuminated through the wide-gap GaAlAsSb layer. The relation between the impact ionization coefficients and the excess noise factor was also discussed. It is clear from Figure 13.47 that the hole ionization coefficient was greater than the electron ionization coefficient and their ratio $\alpha_h/\alpha_e \sim 4$–5. The ionization by holes from the spin-orbit splitting valence band predominated in the range of electric fields $E = (1.5–2.3) \times 10^5$ V/cm.

An example of device structure of InGaAsSb APD with separate absorption and multiplication region, (SAM) APD, is shown in Figure 13.48 [215]. This device is sequentially composed of a 2.2 μm thick Te compensated $Ga_{0.78}In_{0.22}As_{0.18}Sb_{0.82}$ layer with electron concentration $(5–7) \times 10^{15}$ cm^{-3}; a 0.3 μm thick n-$Ga_{0.96}Al_{0.04}Sb$ "resonant" composition layer with electron concentration of 8×10^{16} cm^{-3}; and a 1.5 μm thick $Al_{0.34}Ga_{0.66}As_{0.014}Sb_{0.986}$ window layer with hole concentration of 5×10^{18} cm^{-3}. The location of the p-n junction coincides with the heterointerface between two wide gap materials. The space charge region lies in the n-$Ga_{0.96}Al_{0.04}Sb$/p-$Al_{0.34}Ga_{0.66}As_{0.014}Sb_{0.986}$ heterointerface and results in predominant multiplication of holes in the n-$Ga_{0.96}Al_{0.04}Sb$ multiplication region. The maximum values of the multiplication factor were measured to be $M = 30$–40 at room temperature. The breakdown voltage determined by wide-gap material was about 10–12 V. As a band resonance condition takes place in $Ga_{0.96}Al_{0.04}Sb$ at 0.76 eV, very high values of α_h/α_e ratio up to 60 are achieved. Thus, an essentially unipolar multiplication by holes is provided that reduces the excess noise problem in these APD.
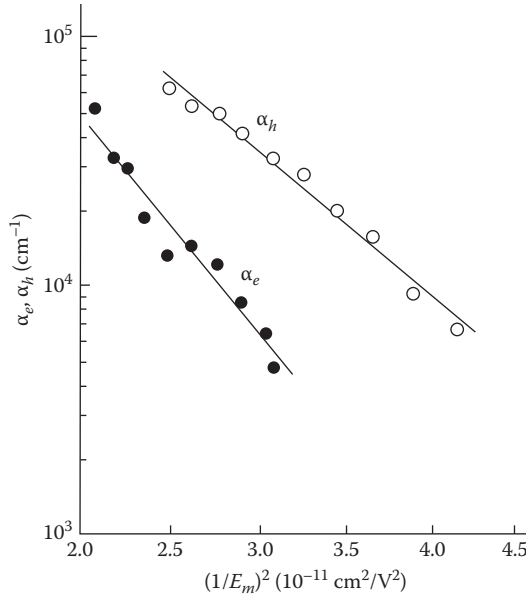
Figure 13.47 Dependence of the hole and electron ionization coefficients on the square of the reciprocal maximum electric field in the $Ga_{0.80}In_{0.20}As_{0.17}Sb_{0.83}$ solid solution at 230 K. (From Andreev, I. A., Mikhailava, M. P., Mel'nikov, S. V., Smorchkova, Yu. P., and Yakovlev, Yu. P., *Soviet Physics-Semiconductor,* 25, 861–65, 1991.)
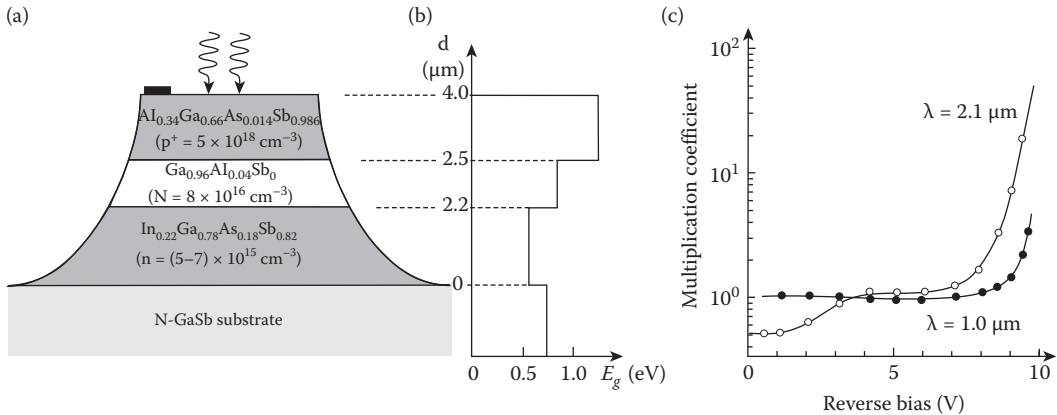
Figure 13.48 SAM APD $Ga_{0.80}In_{0.20}As_{0.17}Sb_{0.83}$ /$Ga_{0.96}Al_{0.04}Sb$ with "resonant" composition in the avalanche region: (a) schematic device structure, (b) band gap structure, and (c) multiplication coefficient versus reverse bias. (From Andreev, I. A., Afrailov, M. A., Baranov, A. N., Marinskaya, N. N., Mirsagatov, M. A., Mikhailova, M. P., Yakovlev, Yu. P., *Soviet Technical Physics Letters,* 15, 692–96, 1989.)

13.5 NOVEL Sb-BASED III-V NARROW GAP PHOTODETECTORS

13.5.1 InTlSb and InTlP

Since an $InAs_{0.35}Sb_{0.65}$ based detector is not sufficient for efficient IR detection operated at lower temperatures in the 8–12 μm range, $In_{1-x}Tl_xSb$ (InTlSb) was proposed as a potential IR material in the LWIR region [217,218]. The TlSb is predicted as a semimetal. By alloying TlSb with InSb, the bandgap of InTlSb could be varied from –1.5 eV to 0.26 eV. Assuming a linear dependence of